Towards in-field and online calibration of inertial navigation systems using moving horizon estimation

Girrbach, Fabian; Zandbergen, Raymond; Kok, Manon; Hageman, Tijmen; Bellusci, Giovanni; DIehl, Moritz

DOI
10.23919/ECC.2019.8796310

Publication date
2019

Document Version
Final published version

Published in
Proceedings of the 18th European Control Conference (ECC 2019)

2019 18th European Control Conference (ECC)
Napoli, Italy, June 25-28, 2019

Towards In-Field and Online Calibration of Inertial Navigation Systems using Moving Horizon Estimation*

Fabian Girrbach[1,2], Raymond Zandbergen[1], Manon Kok[3], Tijmen Hageman[1], Giovanni Bellusci[1], Moritz Diehl[2]

***Abstract*— Inertial sensors are used in an increasing number of autonomous applications. Integrating such sensors into dynamic systems, the problem of their calibration arises naturally. Existing methods often require the sensor to be accurately placed in certain poses, which can be infeasible in practice. In this paper, we present an optimization-based estimator for in-field identification of inertial biases and scale factors. Instead of predefined poses, we use measurements of an accurate global navigation satellite system receiver in the calibration algorithm. By adopting a moving horizon scheme, the resulting estimator has the potential to run on embedded hardware allowing for online calibration without sacrificing robustness. We also present an approach for the simulation of realistic sensor data. The resulting datasets are used to analyze the performance of the optimization-based estimator. The evaluated statistics clearly show that moving horizon estimation improves the robustness and accuracy of the presented calibration approach in the presence of uncertain initial conditions and outperforms traditional recursive filters.**

I. Introduction

Accurate ego-motion tracking is crucial in a number of autonomous applications, e.g., service robotics, autonomous driving or drones. The challenging task of navigating safely through often dynamically changing environments has been addressed in numerous approaches for mapping, localization, *simultaneous localization and mapping* (SLAM), and motion planning [1]. Most navigation systems rely on sensors which allow the localization of the moving system. Typical sensor systems include cameras, LIDAR systems, and *global navigation satellite system* (GNSS) receivers and require some kind of external feedback from the current environment. To increase robustness of pose estimation approaches in scenarios, in which these requirements are not fulfilled, the sensors are combined with inertial sensors. *Inertial measurement unit*s (IMUs) allow to measure angular velocity and acceleration of the system without any dependency on the current environment.

To estimate the pose using acceleration and angular velocity measured by the IMU (see Fig. 1), the sampled measurement data is integrated over time. Small measurement errors and noise contribute to pose errors. To keep the impact of these errors as small as possible the sensors need to be calibrated. Many IMU producers rely on a factory calibration procedure on a chip-level. During system integration, additional stresses or other mechanical influences can affect the previously obtained calibration values making a system-level calibration necessary.

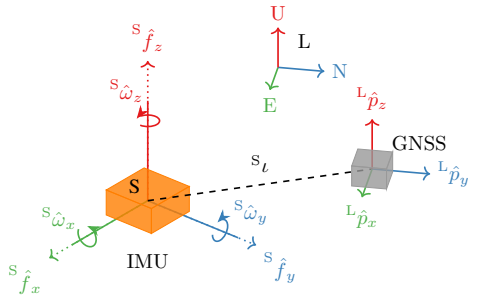

Fig. 1: Schematic drawing showing the measurements of an IMU and RTK-GNSS receiver, respectively. The sensor errors of the accelerometer are visualized by the different lengths (dotted lines) of the measurement axes ${}^{\mathrm{S}}\hat{f}_{x,y,z}$ which can be caused by wrongly calibrated biases ${}^{\mathrm{S}}_{\mathrm{a}}\delta$ and scale factors ${}^{\mathrm{S}}_{\mathrm{a}}\psi$. The lever arm between GNSS antenna and IMU is represented by the dashed line ${}^{\mathrm{S}}\iota$.

Additional information is necessary to identify sensor parameters such as misalignment, nonorthogonality, scale factors, and biases. Common methods make use of predefined poses in which the sensor must be placed with high accuracy. The six-position method [2] requires the inertial system to be mounted on a static and leveled surface with each sensitive axis of every sensor pointing alternately up and down. Alternative methods relax the requirement of special aligned sensor mountings [3] or use a dynamic procedure [4] using a combination of a single-axis rate-table and an attitude change mount to overcome the limitations of static calibration methods. Instead of predefining certain poses, calibration can be also achieved by using additional sensors. In particular the calibration of IMU and camera is a well-studied problem [5]. These methods use a calibration target as reference to track the motion with high accuracy and try to determine calibration and system parameters. Recent advances in GNSS technology allow to obtain very accurate position measurements by compensating

*This work is supported by the project AWESCO (H2020-ITN-642682) funded by the European Union's Horizon 2020 research and innovation program under the Marie Skłodowska-Curie grant agreement No. 642682.

[1] are with Xsens Technologies B.V., 7521 PR Enschede, the Netherlands, firstname.lastname@xsens.com

[2] are with Department of Microsystems Engineering (IMTEK), University of Freiburg, 79110 Freiburg, Germany, firstname.lastname@imtek.uni-freiburg.de

[3] is with Department of Mechanical, Maritime and Materials Engineering, Technical University Delft, 2628 CD Delft, the Netherlands, m.kok-1@tudelft.nl

online for atmospheric errors. This feature is known as *real time kinematics* (RTK) and opens up new possibilities for GNSS-aided technologies such as calibration. The traditional calibration approaches discussed so far are typically solved in a post-processing or smoothing approach, meaning that all the gathered measurement data is used for calibration in a unified approach.

More recently, several filter solutions for online calibration have been proposed which make use of the nonlinear *Kalman filter* (KF) framework [6]–[9]. A drawback of filtering methods is that the estimator is sensitive to initialization and linearization errors, and estimates can diverge if not properly initialized due to the limited amount of information. By using a sliding window of recent measurements, *moving horizon estimation* (MHE) is considered a solution to manage the balancing act between robustness and computation efficiency [10]. In the context of inertial motion tracking, MHE-based estimators [11]–[14] have proven to be an alternative to the widely used *extended Kalman filter*s (EKFs). By considering the online identification of several calibration parameters, we show in this contribution, that MHE is not only a valid alternative, but opens up possibilities beyond state of the art KF approaches.

In this work, we use the measurements of a RTK-GNSS receiver to calibrate scale factors and biases of the IMU sensors. In addition, we account for an unknown lever arm between GNSS antenna and the IMU sensor, which is also estimated. The considered system components are visualized in Fig. 1. We use MHE [10] to estimate the pose and the sensor parameters simultaneously. In contrast to existing post-processing solutions, MHE allows the implementation on embedded devices with limited computational resources, due to its memory-efficient formulation. The presented approach is therefore a step towards in-field and online calibration of GNSS-aided inertial navigation systems. The accuracy with which the parameters can be estimated, depends on the excitation of the system. In order to obtain fairly general results, we adopt a simulation approach to achieve realistic IMU data.

This paper is structured as followed, after defining the considered variables, we define the system dynamics and sensor models in Section II. The optimization-based estimator is formulated in Section III by defining the resulting optimization problem. The established models are further used in Section IV to formulate the optimization-based simulation process of sensor data. The results of the MHE estimator on a set of simulated datasets are discussed in Section V, before we conclude the paper with Section VI.

II. Models

We present an approach to track the motion of a moving system and identify important sensor and system parameters simultaneously. A typical system configuration for inertial navigation is used, consisting of an IMU and a RTK-GNSS receiver. We define the state $\boldsymbol{x}$, parameter $\boldsymbol{p}$, and control $\boldsymbol{u}$ vectors by concatenating of the variables of interest.

$$\boldsymbol{x} = \begin{bmatrix} {}^{\mathrm{L}}p^\top, {}^{\mathrm{L}}v^\top, {}^{\mathrm{LS}}q^\top \end{bmatrix}^\top, \tag{1a}$$

$$\boldsymbol{p} = \begin{bmatrix} {}^{\mathrm{S}}_{\mathrm{a}}\psi^\top, {}^{\mathrm{S}}_{\mathrm{a}}\delta^\top, {}^{\mathrm{S}}_{\mathrm{g}}\psi^\top, {}^{\mathrm{S}}_{\mathrm{g}}\delta^\top, {}^{\mathrm{S}}\iota^\top \end{bmatrix}^\top, \tag{1b}$$

$$\boldsymbol{u} = \begin{bmatrix} {}^{\mathrm{S}}f^\top, {}^{\mathrm{S}}_{\mathrm{LS}}\omega^\top \end{bmatrix}^\top, \tag{1c}$$

where the position ${}^{\mathrm{L}}p \in \mathbb{R}^3$ and velocity ${}^{\mathrm{L}}v \in \mathbb{R}^3$ of the sensor are expressed with respect to the local and non-moving frame L. The orientation between the fixed L and moving sensor frame S is described by the unit quaternion ${}^{\mathrm{LS}}q \in \mathbb{S}^3 \subset \{\mathbb{R}^4 \mid \left\|{}^{\mathrm{LS}}q\right\|^2 = 1\}$ [15]. The sensor and system parameters are collected in $\boldsymbol{p}$. We assume a linear map between the measured signal of the IMU and its physical quantity, where offsets are compensated using the bias terms ${}^{\mathrm{S}}_{\mathrm{a}}\delta, {}^{\mathrm{S}}_{\mathrm{g}}\delta \in \mathbb{R}^3$. The scale factors for accelerometer and gyroscope are defined by ${}^{\mathrm{S}}_{\mathrm{a}}\psi, {}^{\mathrm{S}}_{\mathrm{g}}\psi \in \mathbb{R}^3$ respectively. As an additional system parameter, we include the estimation of the lever arm ${}^{\mathrm{S}}\iota \in \mathbb{R}^3$ between the GNSS antenna and sensor frame S. The control vector $\boldsymbol{u}$ contains the inertial quantities, where ${}^{\mathrm{S}}f, {}^{\mathrm{S}}_{\mathrm{LS}}\omega \in \mathbb{R}^3$ define free acceleration and angular velocity signal observed in the S-frame. Note, that the control signal $\boldsymbol{u}$ is not equal to the measurements obtained by the IMU. The lever arm ${}^{\mathrm{S}}\iota$ is assumed to be constant when expressed with respect to the S frame. Notice that all introduced variables are vector quantities. We use bold symbols to denote concatenated vectors, such as $\boldsymbol{x} \in \mathbb{R}^{10}$, $\boldsymbol{p} \in \mathbb{R}^{15}$, and $\boldsymbol{u} \in \mathbb{R}^6$.

A. Dynamic Model

The dynamics of the motion state $\boldsymbol{x}$ are encoded in an *ordinary differential equation* (ODE) using a conventional point-mass model resulting in expressions

$${}^{\mathrm{L}}\dot{p} = {}^{\mathrm{L}}v, \tag{2a}$$

$${}^{\mathrm{L}}\dot{v} = {R_{\mathrm{LS}}q}\,{}^{\mathrm{S}}f, \tag{2b}$$

$${}^{\mathrm{LS}}\dot{q} = \frac{1}{2}\,{}^{\mathrm{LS}}q \odot \begin{bmatrix} 0 \\ {}^{\mathrm{S}}_{\mathrm{LS}}\omega \end{bmatrix} = \frac{1}{2}\begin{bmatrix} 0 & -{}^{\mathrm{S}}_{\mathrm{LS}}\omega^\top \\ {}^{\mathrm{S}}_{\mathrm{LS}}\omega & {}^{\mathrm{S}}_{\mathrm{LS}}\omega^\times \end{bmatrix}{}^{\mathrm{LS}}q, \tag{2c}$$

where (2a) defines the time derivative of the position ${}^{\mathrm{L}}\dot{p}$. The free acceleration ${}^{\mathrm{S}}f$ is defined in the sensor frame S and needs to be rotated to the L frame to express the time derivative ${}^{\mathrm{L}}\dot{v}$. Notice, that ${}^{\mathrm{LS}}\dot{q}$ depends on the orientation state ${}^{\mathrm{LS}}q$ and the angular velocity ${}^{\mathrm{S}}_{\mathrm{LS}}\omega$, where the $\odot$ operator in (2c) denotes the quaternion multiplication operator which can also be expressed using the skew symmetric matrix ${}^{\mathrm{S}}_{\mathrm{LS}}\omega^\times \in \mathbb{R}^{3\times 3}$.

B. Sensor Models

The ODE (2) is driven by the control input $\boldsymbol{u}$, which is closely related to the IMU measurements. By defining sensor models $h(\boldsymbol{x}, \boldsymbol{u}, \boldsymbol{p})$, we calculate a predicted measurement using the current information about estimated variables $\boldsymbol{x}, \boldsymbol{p}$

and $\boldsymbol{u}$:

$$h_p({}^{\mathrm{L}}p, {}^{\mathrm{LS}}q, {}^{\mathrm{S}}\iota) = {}^{\mathrm{L}}p + R_{{}^{\mathrm{LS}}q}\, {}^{\mathrm{S}}\iota, \tag{3a}$$

$$h_v({}^{\mathrm{L}}v, {}^{\mathrm{LS}}q, {}^{\mathrm{S}}_{\mathrm{LS}}\omega, {}^{\mathrm{S}}\iota) = {}^{\mathrm{L}}v + R_{{}^{\mathrm{LS}}q}[{}^{\mathrm{S}}_{\mathrm{LS}}\omega \times {}^{\mathrm{S}}\iota], \tag{3b}$$

$$h_f({}^{\mathrm{S}}f, {}^{\mathrm{LS}}q, {}^{\mathrm{S}}_{\mathrm{a}}\delta, {}^{\mathrm{S}}_{\mathrm{a}}\psi) = \mathrm{diag}({}^{\mathrm{S}}_{\mathrm{a}}\psi)^{-1}\, {}^{\mathrm{S}}f - {}^{\mathrm{S}}_{\mathrm{a}}\delta + R_{{}^{\mathrm{SL}}q} g, \tag{3c}$$

$$h_\omega({}^{\mathrm{S}}_{\mathrm{LS}}\omega, {}^{\mathrm{S}}_{\mathrm{g}}\delta, {}^{\mathrm{S}}_{\mathrm{g}}\psi) = \mathrm{diag}({}^{\mathrm{S}}_{\mathrm{g}}\psi)^{-1}\, {}^{\mathrm{S}}_{\mathrm{LS}}\omega - {}^{\mathrm{S}}_{\mathrm{g}}\delta, \tag{3d}$$

where time indices have been dropped for notational convenience. To predict a position measurement (3a) from the state variable ${}^{\mathrm{L}}p$, we add the lever arm ${}^{\mathrm{S}}\iota$ by rotating it to the L-frame using $R_{{}^{\mathrm{LS}}q} \in \mathbb{R}^{3\times3}$. A similar relation holds for the velocity measurement in (3b), where we notice a coupling between the IMU and GNSS through the angular velocity ${}^{\mathrm{S}}_{\mathrm{LS}}\omega$. In (3c), we need to compensate for the measured gravitational force $g \in \mathbb{R}^3$ before applying scale factors ${}^{\mathrm{S}}_{\mathrm{a}}\psi$ and biases ${}^{\mathrm{S}}_{\mathrm{a}}\delta$ to the measured acceleration. The identity $R^{-1}_{{}^{\mathrm{LS}}q} = R_{{}^{\mathrm{LS}}q^{-1}} = R_{{}^{\mathrm{SL}}q}$, is used, to express the rotation from L to S-frame, where ${}^{\mathrm{LS}}q^{-1}$ defines the inverse of the quaternion. The linear relation between measured angular velocity of the gyroscope and the control signal ${}^{\mathrm{S}}_{\mathrm{LS}}\omega$ is defined in (3d). It is worth noticing, that the scale factors ${}^{\mathrm{S}}_{\mathrm{a}}\psi, {}^{\mathrm{S}}_{\mathrm{g}}\psi$ can be further used to convert the sensor output to physically relevant SI units.

III. Estimator

The optimization-based estimator uses the system dynamics and the sensor models defined above over an estimation horizon of $N \in \mathbb{N}^+$ measurements. Taking into account that the measurements are acquired at discrete times $t_k \in \mathbb{R}$, we define a discrete-time optimization problem (4) using direct multiple shooting [16]. Eq. (4) states the optimization problem for a specific horizon length N. The horizon is shifted with progressing time so that t_N describes always the current time with the latest available measurement information.

$$\begin{aligned}\min_{\substack{\Delta\boldsymbol{x}_0,\dots,\Delta\boldsymbol{x}_N\\ \Delta\boldsymbol{p}_0,\dots,\Delta\boldsymbol{p}_N\\ \Delta\boldsymbol{u}_0,\dots,\Delta\boldsymbol{u}_{N-1}}} \quad & \frac{1}{2}\left\|\begin{bmatrix}\Delta\boldsymbol{x}_0\\ \Delta\boldsymbol{p}_0\end{bmatrix}\right\|^2_{\mathcal{A}} + \sum_{k=0}^{N-1}\|\boldsymbol{p}_k - \boldsymbol{p}_{k+1}\|^2_{\mathcal{W}}\\ & + \sum_{k=0}^{N-1}\left\|\begin{bmatrix}{}^{\mathrm{S}}\hat{f}_k - h_f(\boldsymbol{x}_k,\boldsymbol{u}_k,\boldsymbol{p}_k)\\ {}^{\mathrm{S}}\hat{\omega}_k - h_\omega(\boldsymbol{u}_k,\boldsymbol{p}_k)\end{bmatrix}\right\|^2_{\mathcal{R}_{\mathrm{IMU}}}\\ & + \sum_{k=0}^{N}\left\|\begin{bmatrix}{}^{\mathrm{L}}\hat{p}_k - h_p(\boldsymbol{x}_k,\boldsymbol{p}_k)\\ {}^{\mathrm{L}}\hat{v}_k - h_v(\boldsymbol{x}_k,\boldsymbol{p}_k)\end{bmatrix}\right\|^2_{\mathcal{R}_{\mathrm{GNSS}}}\end{aligned} \tag{4a}$$

$$\text{s.t.} \quad \boldsymbol{x}_k = \hat{\boldsymbol{x}}_k \boxplus \Delta\boldsymbol{x}_k, \quad k = 0,\dots,N, \tag{4b}$$

$$\boldsymbol{p}_k = \hat{\boldsymbol{p}}_k \boxplus \Delta\boldsymbol{p}_k, \quad k = 0,\dots,N, \tag{4c}$$

$$\boldsymbol{u}_k = \hat{\boldsymbol{u}}_k \boxplus \Delta\boldsymbol{u}_k, \quad k = 0,\dots,N-1, \tag{4d}$$

$$\boldsymbol{x}_{k+1} = \phi(\boldsymbol{x}_k, \boldsymbol{p}_k, \boldsymbol{u}_k), \quad k = 0,\dots,N-1, \tag{4e}$$

where the cost function (4a) consists of four parts. The first line in (4a) defines the arrival cost and the random walk model of the estimated parameters. The arrival cost penalizes the initial increments $\Delta\boldsymbol{x}_0$ and $\Delta\boldsymbol{p}_0$ according to the arrival cost information matrix $\mathcal{A}$ to account for prior or past information. The parameters are modeled as random walk and their jumps between successive $\boldsymbol{p}_k$ and $\boldsymbol{p}_{k+1}$ are penalized according to their random walk standard deviation $\mathcal{W}$. The second and third line in (4a) define the squared residuals between predicted and acquired measurements for each sensor (IMU,GNSS) according to the sensor models (3). Each residual is weighted according to its information matrix $\mathcal{R}_{\mathrm{IMU}}, \mathcal{R}_{\mathrm{GNSS}} \in \mathbb{R}^{6\times6}$ and summed over the horizon N. The constraints (4b)-(4d) establish the relation between increments and states using the $\boxplus$ operator, a generalization of the addition operator, which also holds for quaternions. Notice, that the optimization variables $\Delta\boldsymbol{x}$, $\Delta\boldsymbol{p}$, and $\Delta\boldsymbol{u}$ are increments with respect to initialization values $\hat{\boldsymbol{x}}, \hat{\boldsymbol{p}}, \hat{\boldsymbol{u}}$ of the variables defined in (1). The increments can be also interpreted as error states between initialization and optimal value. We optimize on a valid manifold in $\mathrm{SO}(3)$ by using its Lie Algebra [17]. In order to obtain a closed state trajectory according to the system dynamics, the typical multiple shooting constraints are expressed in (4e) using an integrator function ϕ, which makes use of the ODE of the system (2). The resulting optimization problem for each horizon is solved using a constrained Gauss-Newton algorithm. Before shifting the measurement horizon to the current time, the arrival cost needs to be computed. We adopt a system reduction approach using a Schur complement on the *Karush-Kuhn-Tucker* (KKT) system at the optimal solution $\boldsymbol{x}^*, \boldsymbol{p}^*, \boldsymbol{u}^*$. Notice, that for a horizon length of $N = 1$ the resulting estimator is equal to the *iterated extended Kalman filter* (IEKF) [18], which allows for straight forward comparison of MHE and traditional filtering methods.

IV. Simulator

The results of a calibration procedure which is based on dynamic motion of the system will always depend on the motion trajectory itself. In the trivial case of a static sensor, it is easy to understand that observed measurement errors can be either a result of wrongly calibrated scale factors or biases. Therefore the parameters are not observable in this scenario. To obtain fairly general results, we simulate datasets, which contain randomly generated motion trajectories with various degree of excitation in terms of acceleration and angular velocity changes. Sensor errors can be added to the noise-free data and the true values can be used to assess the performance of the estimator. The simulator uses the same framework for nonlinear optimization as the estimator and employs the same models. We re-use the notation and definitions for state $\boldsymbol{x}$, parameters $\boldsymbol{p}$ and controls $\boldsymbol{u}$. Instead of estimating states and parameters given the controls, we solve an optimal reference tracking with the goal of identifying the necessary controls to track a random trajectory. The entire simulation process is visualized in Fig. 2 and can be summarized by the following steps:

1) A seed value for the random generator is set to achieve a repeatable process.
2) $M \in \mathbb{N}$ waypoints in position and orientation are sampled on a coarse time-grid by drawing samples from the corresponding Gaussian distribution $\breve{\boldsymbol{x}}_{0:M} \sim \mathcal{N}(0, \sigma)$, see Table I.

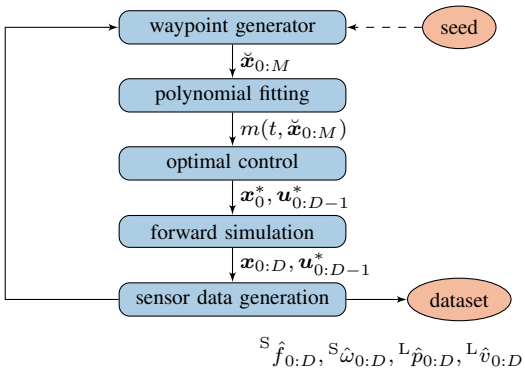

Fig. 2: Flowchart of simulation process to obtain IMU and RTK-GNSS sensor data for random motion trajectories.

3) To achieve a realistic and smooth trajectory, the waypoints are fitted to a polynomial of third order yielding the time-continuous model function $m(t, \breve{\boldsymbol{x}}_{0:M})$.
4) The model equation represents a continuous-time reference trajectory and is used to formulate a discrete optimal reference tracking problem (5) of length $D \in \mathbb{N}$ with sample time $T_{\mathrm{S}} := t_{k+1} - t_k, k = 0, \dots, D-1$.
5) After finding a set of feasible controls $\boldsymbol{u}_{0:D-1}^*$ satisfying the bounds on the controls (5c) and the initial velocity constraints (5e), we simulate the system using the same implicit integrator function $\phi(\boldsymbol{x}_k, \breve{\boldsymbol{p}}, \boldsymbol{u}_k)$ to obtain a state trajectory for the time grid according to the sampling rate of the IMU.
6) Randomly sampled parameter errors $\breve{\boldsymbol{p}} \sim \mathcal{N}(0, \Sigma_{\boldsymbol{p}})$ are used to generate sensor measurements for IMU and RTK-GNSS according to their sensor models defined in (3) from the obtained state $\boldsymbol{x}^*$ and control $\boldsymbol{u}^*$ trajectories. Furthermore, we add white noise to ${}^{\mathrm{S}}\hat{f}_{0:D}, {}^{\mathrm{S}}\hat{\omega}_{0:D}, {}^{\mathrm{L}}\hat{p}_{0:D}, {}^{\mathrm{L}}\hat{v}_{0:D}$.

The optimal control problem solved during simulation can be summarized as follows:

$$\min_{\substack{\boldsymbol{x}_0,\dots,\boldsymbol{x}_D \\ \boldsymbol{u}_0,\dots,\boldsymbol{u}_{D-1}}} \quad \sum_{k=0}^{D} \|\boldsymbol{x}_k - m(t_k, \breve{\boldsymbol{x}}_{0:M})\|_S^2 + \sum_{k=0}^{D-1} \|\boldsymbol{u}_k\|^2 \tag{5a}$$

$$\text{s.t.} \quad \boldsymbol{x}_{k+1} = \phi(\boldsymbol{x}_k, \breve{\boldsymbol{p}}, \boldsymbol{u}_k), \qquad k = 0, \dots, D-1 \tag{5b}$$

$$|\boldsymbol{u}_k| \leq \boldsymbol{u}^{+-}, \qquad k = 0, \dots, D-1 \tag{5c}$$

$$\left\| Z_{{}^{\mathrm{LS}}q} \boldsymbol{x}_D \right\|^2 = 1, \tag{5d}$$

$$\left\| Z_{{}^{\mathrm{L}}v} \boldsymbol{x}_0 \right\|^2 = 0, \tag{5e}$$

$$\breve{\boldsymbol{x}}_{0:M} \sim \mathcal{N}(0, \Sigma_{\boldsymbol{x}}), \qquad M \in \mathbb{N} \tag{5f}$$

where we want to highlight that the parameters $\boldsymbol{p}$ are no longer considered an optimization variable. Apart from the shooting constraints (5b) and the integrator function $\phi(\boldsymbol{x}_k, \breve{\boldsymbol{p}}, \boldsymbol{u}_k)$, we define box constraints on the controls (5c) which take the limited measurement range of the sensors into account. Notice, that we do not make use of increments in this formulation. To ensure a valid manifold in $\mathrm{SO}(3)$, we add an additional equality constraint (5d) which ensures ${}^{\mathrm{LS}}q$ to have unit-norm [19]. The matrices Z in (5d) and (5e) select the corresponding entries in $\boldsymbol{x}$ for the indexed variable to impose the unit-norm constraint on ${}^{\mathrm{LS}}q$ and the zero initial velocity constraint on ${}^{\mathrm{L}}v$.

TABLE I: Simulation parameters in terms of mean μ and standard deviation σ to sample waypoints and sensor errors.

	Parameter	μ	σ	Unit
Waypoints	${}^{\mathrm{L}}p$	0	$[5, 5, 1]^\top$	m
	${}^{\mathrm{LS}}q$	0	60	deg
Accelerometer	${}^{\mathrm{S}}_{\mathrm{a}}\delta$	0	0.125	$\mathrm{m\,s^{-2}}$
	${}^{\mathrm{S}}_{\mathrm{a}}\psi$	0	10	%
Gyroscope	${}^{\mathrm{S}}_{\mathrm{g}}\delta$	0	0.2	$\mathrm{deg\,s^{-1}}$
	${}^{\mathrm{S}}_{\mathrm{g}}\psi$	0	10	%
GNSS	${}^{\mathrm{S}}\iota$	0	$[5, 5, 2.5]^\top$	m
	${}^{\mathrm{L}}\hat{p}$	0	0.05	m
	${}^{\mathrm{L}}\hat{v}$	0	0.3	$\mathrm{m\,s^{-1}}$

TABLE II: Common initialization of navigation states and calibration parameters for both initialization scenarios.

	Parameter	μ	σ	Unit
Navigation	${}^{\mathrm{L}}p_0^{[0]}$	${}^{\mathrm{L}}\hat{p}_0$	${\mathcal{R}_p}^{-1}$	m
	${}^{\mathrm{L}}v_0^{[0]}$	${}^{\mathrm{L}}\hat{v}_0$	${\mathcal{R}_v}^{-1}$	$\mathrm{m\,s^{-1}}$
Acc	${}^{\mathrm{S}}_{\mathrm{a}}\delta_0^{[0]}$	0	0.15	$\mathrm{m\,s^{-2}}$
	${}^{\mathrm{S}}_{\mathrm{a}}\psi_0^{[0]}$	1.0	0.25	
Gyro	${}^{\mathrm{S}}_{\mathrm{g}}\delta_0^{[0]}$	0	0.25	$\mathrm{deg\,s^{-1}}$
	${}^{\mathrm{S}}_{\mathrm{g}}\psi_0^{[0]}$	1.0	0.2	
GNSS	${}^{\mathrm{S}}\iota_0^{[0]}$	0	$[10, 10, 3]^\top$	m

V. Results

In this section, we use 20 simulated datasets generated by following the simulation process described in Section IV. The randomness in the simulated trajectories is introduced by sampling waypoints and sensor calibration errors from normal distributions according to Table I. The IMU measurements are sampled at a frequency of 400 Hz and contain additional white noise according to their noise densities ${}_{\mathrm{a}}\eta = 77.8\ \mu\mathrm{g}\sqrt{\mathrm{Hz}}^{-1}$ and ${}_{\mathrm{g}}\eta = 0.008\ \mathrm{deg\,s^{-1}}\sqrt{\mathrm{Hz}}^{-1}$. For comparison of the estimated results, we save the true simulated values for each motion trajectory and compute the difference between the estimated and ground truth values. To assess the performance and accuracy we evaluate the differences in terms of mean *root mean square error*s (RMSEs) over all 20 datasets for different horizon lengths $N = 1, \dots, 15$. The initialization or equivalently, the formulation of the prior, plays a crucial role in the context of state estimation. Especially the initial guess of the orientation state ${}^{\mathrm{LS}}q_0^{[0]}$ is a major cause of linearization errors in nonlinear estimation approaches, which handle the nonlinearity by finding a linear approximation of the nonlinear system of equations. The prior of the estimator is formulated by defining its mean and

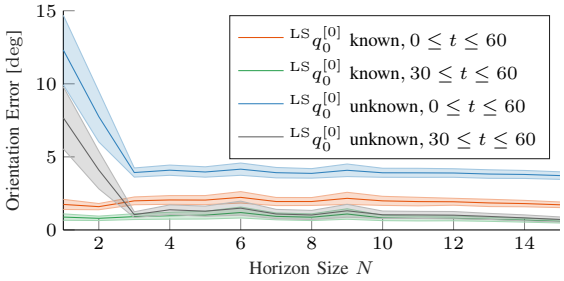

Fig. 3: Comparison of the orientation error for different horizon lengths N using a perfect and an uncertain initial guess. The mean RMSE over all datasets is visualized using the solid line and its standard error using the colored patch.

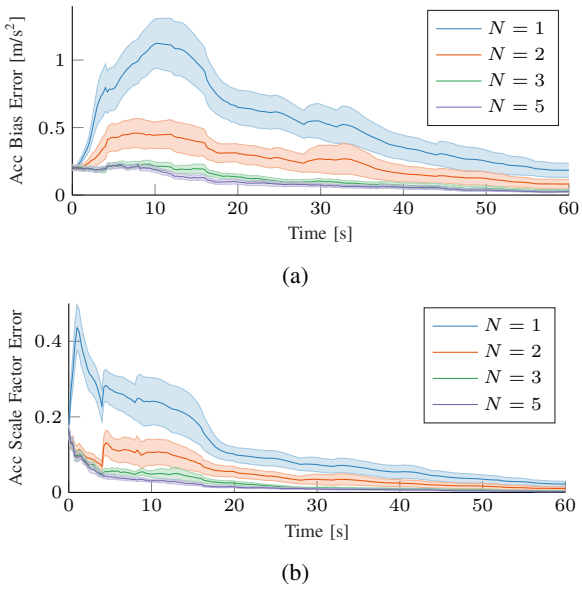

Fig. 4: Evolution of error for estimating accelerometer biases (a) and scale factors (b) over time using an uncertain initial orientation for different horizons lengths N. The mean error over all datasets is visualized using the solid line and the corresponding standard error using the colored patch.

standard deviation and is summarized in Table II. Whereas the navigation states $^{\mathrm{L}}p_0^{[0]}$ and $^{\mathrm{L}}v_0^{[0]}$ are initialized using the GNSS measurements, the orientation state $^{\mathrm{LS}}q_0^{[0]}$ is not directly measured. In practice, the sensor can be either placed in a pose with known orientation or additional sensors such as a magnetometer can be used to determine the initial orientation. Notice that the accuracy of the latter method depends on the calibration of the magnetometer itself, which is a research field of its own [20].

We consider two scenarios: The orientation is either initialized at the true value or assumed to be unknown and set to 0 deg with a large standard deviation of 60 deg. The remaining states are initialized according to Table II for both scenarios. Fig. 3 shows the consequences of the two different initialization methods for different horizon lengths N. If initialized at the true value, we observe a nearly constant orientation error independent of the horizon length N. This behavior can be confirmed by considering the calibration errors in Table III for specific horizons N. With exactly known initial conditions, the mean calibration errors are of same magnitude and converge to similar values after 60 s. In case of an unknown orientation, we observe in Fig. 3, strongly decreasing orientation errors up to a horizon length of $N = 3$ and a constant mean error for horizons $N > 3$. Notice that the plotted mean error does not recover instantly from the wrong initialization by increasing the horizon length, which results in an offset between the two initialization scenarios. When the transient orientation effects are excluded from the evaluation by only considering the last 30 s of the datasets it can be verified that the offset of the mean error is mainly explained by the wrong initialization of orientation and calibration parameters. On the other hand, we obtain higher errors for short horizons $N < 3$ even when considering only the last 50% of the datasets. From this it can be concluded that longer horizons are not only able to handle initialization errors better, but improve estimation in general.

This conclusion is supported by Fig. 4, which shows the evolution of errors over time for accelerometer biases and scale factors for horizons $N = \{1, 2, 3, 5\}$. We notice that for both calibration parameters, a horizon length of $N = 1$ results in errors over time which are multiple times larger than the errors of the initial guess at $t = 0$ s. Apart from the diverging estimates, we also notice that the errors do not converge to a reasonably small values at the end of the simulated calibration procedure at $t = 60$ s. By increasing the horizon $N > 1$, the risk of divergence is clearly decreased even though a desired convergence behavior is only observed for horizons $N \geq 3$, for which the errors decrease continuously with time t. This behavior can be verified by analyzing the mean, maximum, and minimum calibration errors in Table III. The results confirm that increasing the horizon length results in consistently lower maximum errors over the whole 60 s of the datasets in the presence of orientation initialization errors. An assessment of the calibration accuracy at the end of the calibration procedure shows that despite an uncertain and unknown initial orientation, estimators with a horizon size $N \geq 3$ reach a high calibration accuracy. The errors in Table III converge after $t = 60$ s to values similar to those we obtain for the scenario with with known initial orientation.

VI. Conclusion

A MHE-based calibration method for RTK-GNSS-aided inertial navigation systems has been presented, capable of determining biases and scale factors of the inertial sensors and the lever arm between the IMU and the GNSS antenna. The estimator does not require any additional information beside the available measurements and a dynamic excitation of the system itself. To obtain fairly general results from the excitation depending calibration accuracy, a simulation approach for realistic sensor data has been developed to

TABLE III: Estimator Calibration Errors

N	${}^{\mathrm{S}}_{\mathrm{a}}\delta$ [$\mathrm{m\,s^{-2}}$]			${}^{\mathrm{S}}_{\mathrm{g}}\delta$ [$\mathrm{deg\,s^{-1}}$]			${}^{\mathrm{S}}_{\mathrm{a}}\psi$ [10^{-2}]			${}^{\mathrm{S}}_{\mathrm{g}}\psi$ [10^{-2}]			${}^{\mathrm{S}}\iota$ [m]		
	mean	max	min	mean	max	min	mean	max	min	mean	max	min	mean	max	min
Initial ${}^{\mathrm{L}}_{\mathrm{S}}q_0$ known; $0 \leq t \leq 60$															
1	0.125	0.248	0.057	0.163	0.323	0.092	3.427	9.039	**1.803**	5.195	12.915	2.055	1.547	3.373	0.46
5	**0.117**	**0.198**	**0.052**	**0.155**	**0.238**	**0.058**	**3.154**	**5.503**	1.932	**5.352**	**9.671**	**1.579**	**1.325**	**3.1**	**0.344**
Initial ${}^{\mathrm{L}}_{\mathrm{S}}q_0$ known; $t = 60$															
1	0.024	0.072	**0.005**	**0.033**	**0.085**	**0.007**	0.281	0.906	0.048	0.31	0.897	**0.056**	0.098	0.321	0.021
5	**0.022**	**0.056**	0.006	**0.033**	0.086	**0.007**	**0.218**	**0.731**	**0.023**	**0.246**	**0.735**	0.058	**0.07**	**0.313**	**0.011**
Initial ${}^{\mathrm{L}}_{\mathrm{S}}q_0$ unknown; $0 \leq t \leq 60$															
1	0.648	1.941	0.155	0.559	1.362	0.193	16.255	55.482	3.141	22.711	71.166	5.922	3.29	9.179	0.559
3	0.14	0.35	**0.042**	0.169	0.275	0.064	4.001	10.124	**1.92**	5.923	12.561	1.92	1.665	5.518	0.552
5	**0.125**	**0.234**	0.053	**0.163**	**0.257**	**0.062**	**3.422**	**6.763**	1.959	**5.613**	**11.199**	**1.714**	**1.44**	**3.98**	**0.331**
Initial ${}^{\mathrm{L}}_{\mathrm{S}}q_0$ unknown; $t = 60$															
1	0.184	0.781	0.01	0.085	0.416	0.022	2.222	13.071	0.199	2.515	6.663	0.091	1.282	7.637	0.111
3	0.031	0.208	**0.004**	0.035	**0.087**	**0.005**	0.345	2.373	0.034	0.358	2.437	0.062	0.221	2.596	0.02
5	**0.025**	**0.085**	0.005	**0.034**	0.089	0.009	**0.269**	**1.027**	**0.026**	**0.285**	**0.749**	**0.057**	**0.129**	**1.308**	**0.013**

generate a set of 20 random datasets. By setting the horizon length of the estimator to $N = 1$, we obtain a recursive estimator equal to an IEKF formulation. It has been shown that such traditional filtering methods are prone to diverge over time in the presence of an uncertain initial state. In particular during the first 20 s, the calibration results show large errors, which are drastically decreased by an increase of the horizon length. The optimal estimation behavior and accuracy is achieved for a horizon length of $N \geq 3$, for which the estimators showed high robustness against divergence and recovered fully from the initialization errors.

For the purpose of online and in-field calibration, a direction for future work is to increase the computational efficiency of the developed algorithm by considering the most recent advances in numerical methods which would allow the use of this approach on embedded devices with constrained computational resources.

ACKNOWLEDGMENT

We would like to thank Dr. Jeroen D. Hol for his advise and guidance during his time at Xsens Technologies B.V..

REFERENCES

[1] R. Siegwart, I. R. Nourbakhsh, and D. Scaramuzza, *Introduction to Autonomous Mobile Robots*, 2nd ed. The MIT Press, 2011.

[2] D. Titterton and J. Weston, *Strapdown Inertial Navigation Technology*. IET, 2004.

[3] Z. F. Syed, P. Aggarwal, C. Goodall, X. Niu, and N. El-Sheimy, "A new multi-position calibration method for MEMS inertial navigation systems," *Measurement Science and Technology*, vol. 18, no. 7, pp. 1897–1907, 2007.

[4] D. Lee, S. Lee, S. Park, and S. Ko, "Test and error parameter estimation for MEMS-based low cost IMU calibration," *International Journal of Precision Engineering and Manufacturing*, vol. 12, no. 4, pp. 597–603, 2011.

[5] J. Rehder and R. Siegwart, "Camera/IMU calibration revisited," *IEEE Sensors Journal*, vol. 17, no. 11, pp. 3257–3268, June 2017.

[6] M. D. Shuster, D. M. Chitre, and D. P. Niebur, "In-flight estimation of spacecraft attitude sensor accuracies and alignments," *Journal of Guidance, Control, and Dynamics*, vol. 5, no. 4, pp. 339–343, 1982.

[7] T. Beravs, J. Podobnik, and M. Munih, "Three-axial accelerometer calibration using Kalman filter covariance matrix for online estimation of optimal sensor orientation," *IEEE Transactions on Instrumentation and Measurement*, vol. 61, no. 9, pp. 2501–2511, 2012.

[8] M. E. Pittelkau, "Kalman filtering for spacecraft system alignment calibration," *Journal of Guidance, Control, and Dynamics*, vol. 24, no. 6, pp. 1187–1195, 2001.

[9] W. T. Fong, S. K. Ong, and A. Y. C. Nee, "Methods for in-field user calibration of an inertial measurement unit without external equipment," *Measurement Science and Technology*, vol. 19, no. 8, 2008.

[10] J. B. Rawlings, "Moving horizon estimation," in *Encyclopedia of Systems and Control*. Springer London, 2013, pp. 1–7.

[11] T. Polóni, B. Rohal-Ilkiv, and T. A. Johansen, "Moving horizon estimation for integrated navigation filtering," *IFAC-PapersOnLine*, vol. 48, no. 23, pp. 519–526, 2015.

[12] A. Sveier and O. Egeland, "Pose estimation using dual quaternions and moving horizon estimation," *IFAC-PapersOnLine*, vol. 51, no. 13, pp. 186–191, 2018.

[13] F. Girrbach, J. D. Hol, G. Bellusci, and M. Diehl, "Optimization-based sensor fusion of GNSS and IMU using a moving horizon approach," *Sensors*, vol. 17, no. 5, p. 1159, 2017.

[14] J. Vandersteen, M. Diehl, C. Aerts, and J. Swevers, "Spacecraft attitude estimation and sensor calibration using moving horizon estimation," *Journal of Guidance, Control, and Dynamics*, vol. 36, no. 3, pp. 734–742, 2013.

[15] M. D. Shuster, "Survey of attitude representations," *Journal of the Astronautical Sciences*, vol. 41, pp. 439–517, 1993.

[16] H. Bock and K. Plitt, "A multiple shooting algorithm for direct solution of optimal control problems," *IFAC Proceedings Volumes*, vol. 17, no. 2, pp. 1603–1608, jul 1984.

[17] M. Bloesch, H. Sommer, T. Laidlow, M. Burri, G. Nützi, P. Fankhauser, D. Bellicoso, C. Gehring, S. Leutenegger, M. Hutter, and R. Siegwart, "A primer on the differential calculus of 3D orientations," *CoRR*, vol. abs/1606.05285, 2016.

[18] D. P. Bertsekas, "Incremental least squares methods and the extended Kalman filter," *SIAM Journal on Optimization*, vol. 6, no. 3, pp. 807–822, aug 1996.

[19] F. Girrbach, J. D. Hol, R. Zandbergen, R. Verschueren, G. Bellusci, and M. Diehl, "On the effect of stabilization methods for quaternion invariants on the uncertainty in optimization-based estimation," *IFAC-PapersOnLine*, 2018, in press.

[20] M. Kok, J. D. Hol, T. B. Schön, F. Gustafsson, and H. Luinge, "Calibration of a magnetometer in combination with inertial sensors," in *Proc. of the 15th International Conference on Information Fusion (FUSION)*, July 2012, pp. 787–793.